Wide-Angle Foveation for All-Purpose Use

Sota Shimizu, *Member, IEEE*

***Abstract*—This paper proposes a model of a wide-angle space-variant image that provides a guide for designing a fovea sensor. First, an advanced wide-angle foveated (AdWAF) model is formulated, taking all-purpose use into account. This proposed model uses both Cartesian (linear) coordinates and logarithmic coordinates in both planar projection and spherical projection. Thus, this model divides its wide-angle field of view into four areas, such that it can represent an image by various types of lenses, flexibly. The first simulation compares with other lens models, in terms of image height and resolution. The result shows that the AdWAF model can reduce image data by 13.5%, compared to a log-polar lens model, both having the same resolution in the central field of view. The AdWAF image is remapped from an actual input image by the prototype fovea lens, a wide-angle foveated (WAF) lens, using the proposed model. The second simulation compares with other foveation models used for the existing log-polar chip and vision system. The third simulation estimates a scale-invariant property by comparing with the existing fovea lens and the log-polar lens. The AdWAF model gives its planar logarithmic part a complete scale-invariant property, while the fovea lens has 7.6% error at most in its spherical logarithmic part. The fourth simulation computes optical flow in order to examine the unidirectional property when the fovea sensor by the AdWAF model moves, compared to the pinhole camera. The result obtained by using a concept of a virtual cylindrical screen indicates that the proposed model has advantages in terms of computation and application of the optical flow when the fovea sensor moves forward.**

***Index Terms*—Active sensing, all-purpose use, biomimetics, fovea sensor, image processing, wide-angle foveation (WAF).**

I. Introduction

A FOVEA sensor, which is inspired from the density of cone cells of the human retina is quite applicable for all-purpose use in sensing systems. It gives us a foveated space-variant image as the resolution is the highest in the central field of view (FOV) and gets lower rapidly toward the periphery. Thus, the fovea sensor uses a wide-angle FOV entirely and the central FOV locally in detail by drastically reducing the data in the periphery [1]. Log-polar mapping is often used for a model of the foveated image. The log-polar mapping is inspired by an analytic formulation from biological observation of the primate visual system [2]. Sandini and Tagliasco have applied it to computer vision computationally [3], and his group and other researchers have advanced this model to produce the log-polar vision chip by charge-coupled (CCD) or CMOS technologies [4]–[6]. The log-polar mapping is not only effective for drastic image data reduction (as the human retina does) but also suitable for generating geometrical rotation and scale-invariant feature easily. The latter seems to be one of the most indispensable advantages [4].

As another method to acquire the foveated image, the use of a special wide-angle lens is also well known [7]–[9]. This usually combines the special-made wide-angle foveated (WAF) lens with a commercially available conventional Cartesian (linear) vision chip, where photosensitive elements are arranged uniformly in an array structure. On the other hand, the former approach combines a conventional lens with a log-polar chip, where the size of a photosensitive element is uniform in "fovea," but it changes logarithmically in the "periphery." The author has taken the latter approach, using the actual WAF lens [9], [10]. Many industrial applications of vision sensing require the wide-angle FOV and high resolution at the same time, for image processing, surveillance, and monitoring [11]–[13]. However, almost all of them just use a narrow-angle image sensor with pan–tilt/zoom control or a wide-angle image sensor without sufficient resolution. It seems that the latter approach has a stronger advantage than the former when the fovea sensor is designed by combining multiple coordinate systems. One of the further advantages is that the latter can give us much higher resolution in the central FOV, because the lens enlarges its image optically, when both approaches have the same FOV, i.e., the view angle and the same number of pixels.

Another wide-angle fovea lens by Kuniyoshi (K lens) is known as a model that combines planar projection and spherical projection [8]. This lens achieves foveation by distorting a part of the spherical projection using a logarithmic curve in order to bridge *Cartesian* (*linear*) *planar* projection and *Cartesian spherical* projection. This *spherical logarithmic* part gives us only an approximated log-polar mapped image with a rotation- and scale-invariant (RS-invariant) property. Intuitively, this concept is reasonable, but it seems that this model still has a space to be improved in terms of determining boundaries of the above logarithmic part (concretely, if incident angles corresponding to these boundaries are too large, they cause geometric deformation in the log-polar mapped image). Section II of this paper proposes an advanced wide-angle foveated (AdWAF) model used for designing a fovea sensor for all-purpose use [9]. This proposed model has four areas in its FOV: by combining both Cartesian coordinates and logarithmic coordinates with both the planar projection and the spherical projection (i.e., this model has a planar logarithmic part, in addition to the three areas of the K lens). It should be remarked that the AdWAF model represents images quite flexibly because it includes four types of curve. It covers not only the K lens and other fovea sensors but also various types of lenses (e.g., pinhole camera lens, fish-eye (FE) lens, and log-polar lens).

Manuscript received January 8, 2008; revised May 24, 2008. Current version published October 8, 2008. Recommended by Technical Editor I-M. Chen. This work was supported in part by the Wind and Biomass Energy R&D and Information Center and in part by the Japan Society for the Promotion of Science under a grant.

The author was with the Division of Applied Science and Engineering, California Institute of Technology, Pasadena, CA 91125 USA. He is now with the Advanced Research Institute for Science and Engineering, Waseda University, Tokyo 162-0044, Japan (e-mail: sato@caltech.edu).

Color versions of one or more of the figures in this paper are available online at http://ieeexplore.ieee.org.

Digital Object Identifier 10.1109/TMECH.2008.2002884

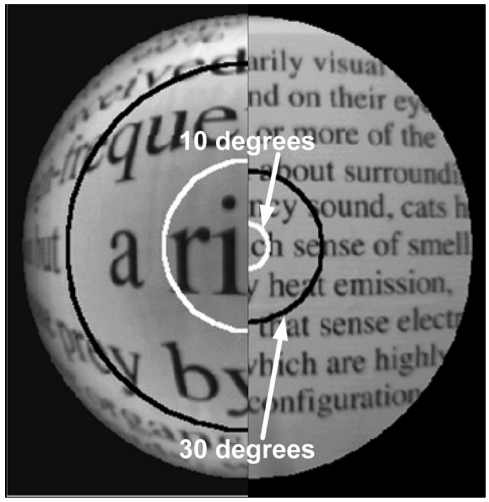

Fig. 1. Comparison of an input image by the existing WAF lens (left half) and the PHC lens image (right half).

Section III of this paper compares the AdWAF model with other foveation models by Sandini's model [3], Bolduc's model [14], and the K lens model, discussing about its flexibility of representation. Further, this section examines the unidirectional property of the AdWAF model, i.e., the proposed model gives the RS-invariant property to its *planar* and *spherical logarithmic* parts and the translation-invariant property to its *planar Cartesian* part, respectively. The scale-invariant property is estimated in comparison with the K lens and the log-polar lens. Moreover, this section examines optical flow of the AdWAF model and the pinhole camera when the camera moves. A concept of virtual cylindrical screen (VCS) is introduced in order to examine the advantages of computation and application of the optical flow by the proposed model when the fovea sensor moves forward.

II. Advanced Wide-Angle Foveated Model

A. Modeling

Fig. 1 compares an input image by the existing WAF lens with the pinhole camera (PHC) lens image. The PHC image assumes to have the same field of view (FOV), i.e., the same view angle and the same number of pixels. This prototype WAF lens realizes about 120° wide-angle FOV and an adequate high resolution in the central FOV at the same time, by distorting the image largely. Thus, the WAF lens is applicable for various levels of image processing (e.g., high-level task: pattern recognition in the central FOV; low-level task: motion detection in the peripheral FOV), i.e., for all-purpose use. This prototype provides a foveated image easily by being attached with the commercially available imaging device such as a CCD camera.

In order to make better all-purpose use of the WAF image, the author defines a geometrical model, namely, an AdWAF model. Fig. 2 shows a sketch of a camera model that combines planar projection and spherical projection. The former is a perspective projection, i.e., linear to the tangent of incident angle (θ) to the lens optical center, and the latter is linear to θ. The AdWAF model is denoted by the following equations, as a function of image height r in terms of θ, combining both planar projection and spherical projection with both Cartesian (linear) coordinates and logarithmic coordinates:

$$\text{if } 0 \le \theta \le \theta_0, \quad r = r_{\max} c_0 f_1 \tan\theta \tag{1}$$

$$\text{else if } \theta_0 \le \theta \le \theta_1, \quad r = r_{\max}\{c_1 \log_a(f_1 \tan\theta) + d_1\} \tag{2}$$

$$\text{else if } \theta_1 \le \theta \le \theta_2, \quad r = r_{\max}\{c_2 \log_b(f_2\theta) + d_2\} \tag{3}$$

$$\text{else if } \theta_2 \le \theta \le \theta_{\max}, \quad r = r_{\max}(c_3 f_2 \theta + d_3) \tag{4}$$

where f_1 and f_2 are focal lengths to the projection plane and the spherical projection surface, respectively; $r_{\max}$ is the maximum image height when $\theta = \theta_{\max}$, $c_i \in (i = 0,\ 1,\ 2,\ 3)$ is a scale modification factor for adjusting the image height partly in each section of the θ, and $d_i \in (i = 1,\ 2,\ 3)$ is a boundary between the sections denoted by

$$d_1 = c_0 f_1 \tan\theta_0 - c_1 \log_a(f_1 \tan\theta_0) \tag{5}$$

$$d_2 = c_1 \log_a(f_1 \tan\theta_1) - c_2 \log_b(f_2\theta_1) + d_1 \tag{6}$$

$$d_3 = c_2 \log_b(f_2\theta_2) - c_3 f_2 \theta_2 + d_2. \tag{7}$$

Because (1)–(4) are continuous at each boundary, if these derivatives are also continuous when $c_0 = c_1 = c_2 = c_3 = 1$,

$$f_1 = \frac{1}{\tan\theta_0} \Bigg/ \left\{ 1 + \log\frac{\tan\theta_1}{\tan\theta_0} + \frac{\theta_1}{\cos\theta_1 \sin\theta_1}\left(\frac{\theta_{\max} - \theta_2}{\theta_2} + \log\frac{\theta_2}{\theta_1}\right)\right\} \tag{8}$$

$$f_2 = \frac{f_1 \tan\theta_0}{\cos\theta_1 \sin\theta_1}\frac{\theta_1}{\theta_2} \tag{9}$$

$$a = \exp\left(\frac{1}{f_1 \tan\theta_0}\right) \tag{10}$$

$$b = \exp\left(\frac{1}{f_2\theta_2}\right). \tag{11}$$

The AdWAF model divides the FOV into four regions, i.e., fovea ($0 \le \theta \le \theta_0$), para-fovea ($\theta_0 \le \theta \le \theta_1$), near-periphery ($\theta_1 \le \theta \le \theta_2$), and periphery ($\theta_2 \le \theta \le \theta_{\max}$). The fovea is planar and its image height is linear to the object height h. On the other hand, the periphery is spherical and its image height is linear to the incident angle θ. Fig. 3 simulates images remapped by the AdWAF model and the PHC lens model (in condition that the boundaries of FOV, $\theta_0,\ \theta_1,\ \theta_2,$ and $\theta_{\max}$ are 9.826°, 19.107°, 34.715°, and 60°) respectively. The intensity is changed in order to see each boundary easily. Note that the AdWAF model is applicable not only for software methods, i.e., resampling data computationally as shown in Fig. 3(a), but also for hardware design of inputting/outputting device, e.g., a fovea sensor such as the WAF lens.

Fig. 4 shows the image height r, magnifications dr/dh and r/h in the radial and tangential directions of the AdWAF model, versus the object height h. The $h_{\max}$ and $r_{\max}$ are normalized to 1 (when $\theta_{\max} = 60°$) in order to compare other types of lenses, i.e., a log-polar (LP) lens, a fish-eye (FE) lens, the PHC lens, and the WAF lens. In this simulation, the boundaries of FOV, i.e.,

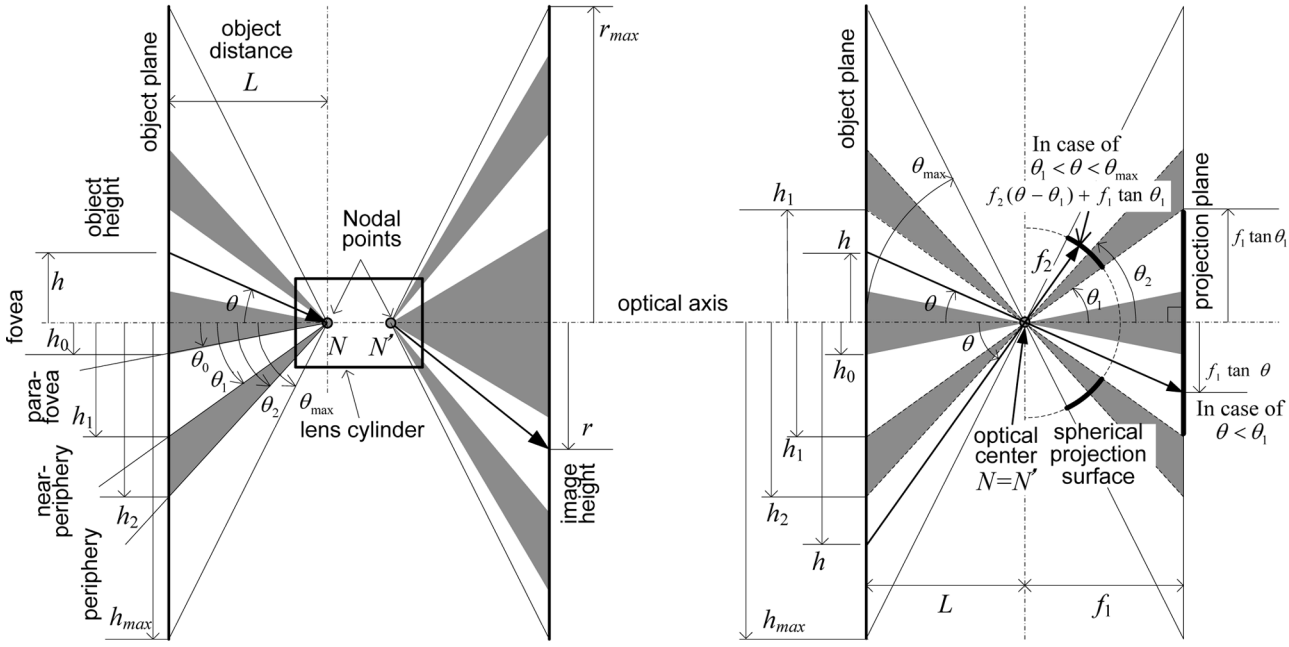

Fig. 2. Camera model based on combination of planar projection and spherical projection.

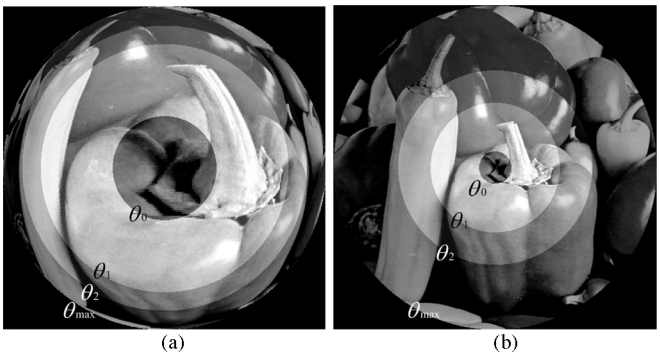

Fig. 3. Comparison of (a) AdWAF image and (b) PHC lens image.

h_0, h_1, and h_2, are 0.1 ($\theta_0 = 9.826°$), 0.4 ($\theta_1 = 19.107°$), and 0.6 ($\theta_2 = 34.715°$), respectively. Each type of lens is defined in the following.

LP lens:

$$\text{if } 0 \le \theta \le \theta_0 \text{ (fovea)}, \qquad r = r_{\max} f_{\mathrm{lp}} \tan\theta \tag{12}$$

$$\text{else if } \theta_0 \le \theta \le \theta_{\max} \in \text{(periphery)},$$

$$r = r_{\max}\left\{\log_{a_{\mathrm{lp}}}(f_{\mathrm{lp}} \tan\theta) + d_{\mathrm{lp}}\right\} \tag{13}$$

where d_{lp} is denoted as

$$d_{\mathrm{lp}} = f_{\mathrm{lp}} \tan\theta_0 - \log_{a_{\mathrm{lp}}}(f_{\mathrm{lp}} \tan\theta_0) \tag{14}$$

a focal length f_{lp} is denoted as

$$f_{\mathrm{lp}} = \frac{1}{\{1 + \log(\tan\theta_{\max}/\tan\theta_0)\}\tan\theta_0} \tag{15}$$

a basis a_{lp} is denoted as

$$a_{\mathrm{lp}} = \exp\left(\frac{1}{f_{\mathrm{lp}} \tan\theta_0}\right) \tag{16}$$

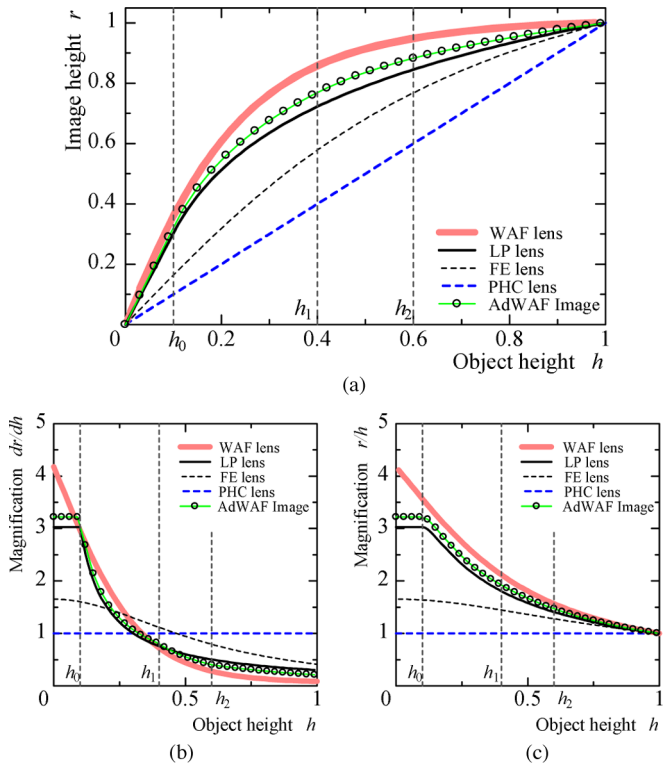

Fig. 4. Comparison of the AdWAF model and other types of lens. (a) Image height r. (b) Magnification (in radial). (c) Magnification (in tangential).

such that (12) and (13) are continuous at $\theta = \theta_0$, and their derivatives are also continuous. Note that the LP lens is equivalent to the AdWAF model when $\theta_1 = \theta_2 = \theta_{\max}$, $c_0 = c_1 = 1$, and $c_2 = c_3 = 0$. Its fovea and "periphery" correspond to the fovea and para-fovea of the AdWAF model, respectively.

FE lens:

$$r = \frac{r_{\max}}{\theta_{\max}}\theta, \qquad 0 \le \theta \le \theta_{\max}. \tag{17}$$

PHC lens:

$$r = \frac{r_{\max}}{\tan\theta_{\max}}\tan\theta, \qquad 0 \le \theta \le \theta_{\max}. \tag{18}$$

WAF lens:

$$r = r_{\max}(a_0\theta^3 + a_1\theta^2 + a_2\theta), \qquad 0 \le \theta \le \theta_{\max}. \tag{19}$$

A bold solid line shows the actual WAF lens [7]. The distribution of its image height and magnification is characterized by the design concept of the WAF lens, i.e., acquiring a wide FOV and high resolution in the central FOV. Its magnification in the radial direction is much higher than the PHC lens (a bold broken line) and the FE lens (a fine broken line) in small incident angles. On the other hand, it is lower in large incident angles. This figure shows that the AdWAF model (a fine solid line with circles) can acquire a higher magnification in the fovea $0 \le h \le h_0$ (i.e., $0 \le \theta \le \theta_0$) than the LP lens (a solid line), in case of the same FOV. The scale modification factor c_i is applicable for adjusting the image height of the AdWAF image in order to make its magnification in the fovea equal to that of the LP lens. If $c_0 = c_1 = c_2 = c_3 = 0.93$, the modified magnification is nearly equal to that of the LP lens in the fovea in case of Fig. 4(b). This means that the AdWAF model can reduce the number of pixels by 13.5% in the whole of image compared to the LP lens.

B. Implementation

Fig. 5 shows that the AdWAF image is simulated by the proposed model, compared to other types of lens, by the whole view, in condition of $r_{\max} = 64$ pixel, $\theta_{\max} = 60°$, $\theta_0 = 9.826°$, $\theta_1 = 19.107°$, and $\theta_2 = 34.715°$. Each image is simulated from a Cartesian target image of 512×512 pixels [see Fig. 5(a)]. It is obvious that the AdWAF image [see Fig. 5(f)] has a higher resolution in its central area than the LP lens image [see Fig. 5(c)]. On the other hand, the resolution of its peripheral area is between those of the WAF lens and the LP lens. It should be remarked that all of these simulated images can be represented using the AdWAF model.

Fig. 6 shows the AdWAF image actually extracted from the WAF lens in the same condition as in Fig. 5. Fig. 6(a)–(d) is an actual input image by the WAF lens, the extracted AdWAF image by the whole view, the para-fovea image, i.e., a log-polar image (with "planar" logarithmic coordinates) by (4), and the fovea image (with *planar Cartesian* coordinates) by (3), respectively. The AdWAF image has not only a wide FOV but also the rotation- and scale-invariant property in the para-fovea and translation-invariant property in the fovea; thus, it is quite suitable for all-purpose use.

Fig. 5. Simulated images of the WAF lens, LP lens, FE lens, PHC lens, and AdWAF model. (a) Cartesian target image (of 512×512 pixels). (b) WAF lens image. (c) LP lens image. (d) FE lens image. (e) PHC lens image. (f) AdWAF image.

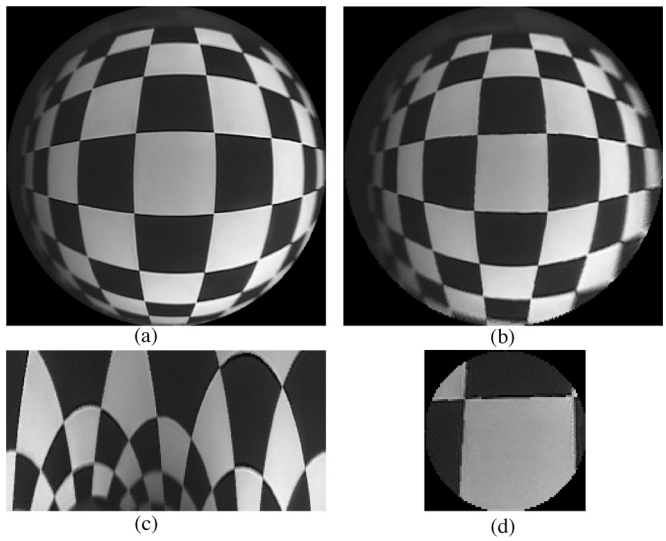

Fig. 6. AdWAF image extracted from an actual image by the WAF lens. (a) Actual image by WAF lens. (b) Whole view of the AdWAF image. (c) Para-fovea image. (d) Fovea image.

III. Examination

A. Generalization of Representing Log-Polar Sensor

Generally, an AdWAF model can represent other foveation models including log-polar mapping. For example, foveation

models used for the existing log-polar chip and vision system [3], [14] are represented by the AdWAF model in condition of $\theta_1 = \theta_2 = \theta_{\max}$ and $c_2 = c_3 = 0$. The FOV of such models is divided into fovea and "periphery," similarly to the LP lens. The following discussion assumes to represent the FOV using Cartesian coordinates for comparison. The para-fovea of the AdWAF model denotes a log-polar grid in a part of the "periphery." The log-polar grid is composed of rings and rays for the position of receptive fields (RFs), as shown in Fig. 7(b) and (c). On the other hand, the fovea has uniform size of the RFs. This size is equal to that of the first ring in the "periphery," in order to avoid discontinuity at the fovea/periphery boundary. The radius of each ring is calculated as the normalized object height h using the AdWAF model as follows:

$$\text{if } 0 \le \theta \le \theta_0 \text{ (fovea)}, \qquad h = \frac{r}{r_{\max} c_0 f_1 \tan\theta_{\max}} \tag{20}$$

$$\text{else if } \theta_0 \le \theta \le \theta_{\max} \text{ ("periphery")}, \qquad h = \frac{\tan\theta_0}{\tan\theta_{\max}} a^{(r-r_0)/r_{\max} c_1} \tag{21}$$

where r_0 is the radius of the fovea/periphery boundary, i.e.,

$$r_0 = r_{\max} c_0 f_1 \tan\theta_0. \tag{22}$$

With respect to the log-polar sensor, one of the most remarkable differences between the lens and the existing solid-state chip is the number N of the RFs along the ring. Here, the case of the lens assumes that each photosensitive element is equivalent to the RF. The number N of the LP lens always increases, as h gets larger (in proportion to r), while the log-polar chip has a constant number N_0 in the "periphery." Fig. 7(a) compares N in both cases versus h, when $N_0 = 128$, $\theta_0 = 9.826°$, $\theta_{\max} = 60.0°$, and $c_0 = c_1 = 1$, in addition to the condition when the number of RFs is equal in the fovea.

Comparing Sandini's model [see Fig. 7(b)] and Bolduc's model [see Fig. 7(c)], although N_0, θ_0, and $\theta_{\max}$ are common between these two models, the size of RFs changes differently in a hatched area of the FOV (i.e., "periphery"). This means that a ring number is not equal to the image height r, necessarily, because each RF could be composed of multiple photosensitive elements. The AdWAF model represents different arrangements of the log-polar grid by the scale modification factors c_0 and c_1. The factor c_0 modifies r_0 (i.e., it modifies the number of RFs in the fovea). The variable c_1 adjusts exponential change of a radius of the ring. In this case, r in (20) and (21) can be regarded as the ring number. Thus, c_0 and c_1 fit both the models into the AdWAF model even with the same N_0, θ_0, and $\theta_{\max}$.

It is noted that the AdWAF model represents a combination of the FE lens and the log-polar chip, if the FE lens is approximated well as the PHC lens model within θ_0 (i.e., in the fovea). Note that this case assumes $\theta_2 = \theta_{\max}$ and $c_3 = 0$.

A model of another wide-angle fovea lens by Kuniyoshi (K lens) [8] has a *planar Cartesian* part in $0 \le \theta \le \theta_0$, a *spherical logarithmic* part in $\theta_0 \le \theta \le \theta_1$, and a *spherical Cartesian* part in $\theta_1 \le \theta \le \theta_{\max}$, but it does not have the planar logarithmic part [para-fovea by (2)]. Thus, the AdWAF model represents

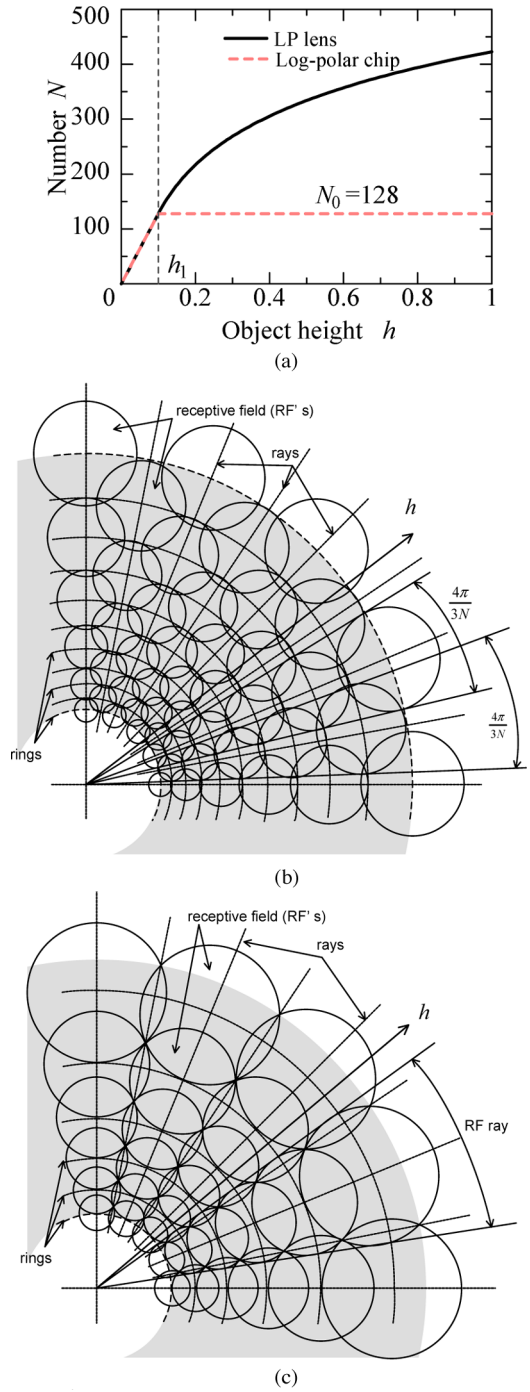

Fig. 7. Foveation models of the LP lens log-polar chip. (a) Number N of the RFs along the ring versus θ. (b) Sandini's pseudotriangular model when $N_0 = 16$. (c) Bolduc's circular model when $N_0 = 16$.

the K lens model, in condition of $f_{k_1} = f_1$ and $f_{k_2} = f_2$, as follows.

K lens model:

$$\text{if } 0 \le \theta \le \theta_0, \quad r = r_{\max} f_{k1} \tan\theta \tag{23}$$

$$\text{else if } \theta_0 \le \theta \le \theta_1, \quad r = r_{\max} \left\{ \log_{b_k} (f_{k2}\theta) - p \right\} \tag{24}$$

$$\text{else if } \theta_1 \le \theta \le \theta_{\max}, \quad r = r_{\max} (f_{k2}\theta + q) \tag{25}$$

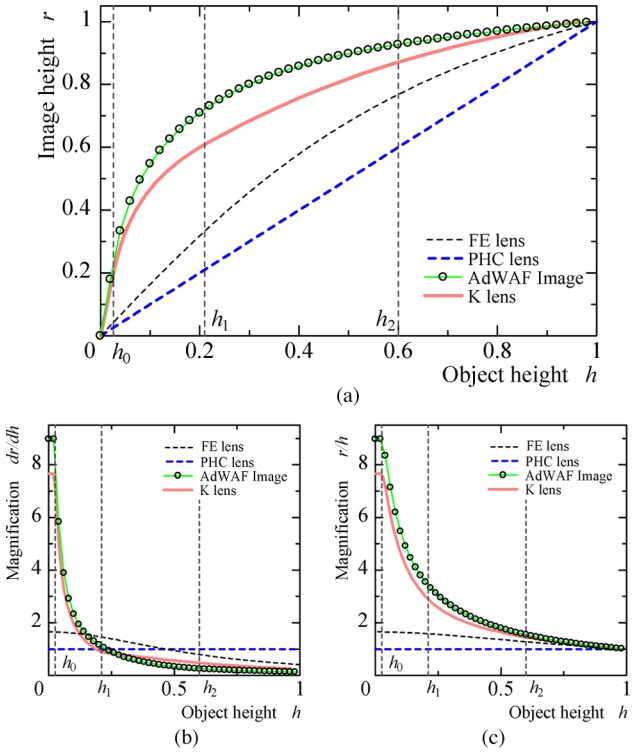

Fig. 8. Comparison of the AdWAF image and the K lens. (a) Image height r. (b) Magnification (in radial). (c) Magnification (in tangential).

where

$$b_k = \exp\left\{\frac{1}{1 - f_{k1}\tan\theta_0}\left(\frac{\theta_{\max} - \theta_1}{\theta_1} + \log\frac{\theta_1}{\theta_0}\right)\right\} \quad (26)$$

$$p = \log_{b_k}(f_{k2}\tan\theta_0) - f_{k1}\tan\theta_0 \quad (27)$$

$$q = -f_{k2}\theta_1 + \log_{b_k}\frac{\theta_1}{\theta_0} + f_{k1}\tan\theta_0. \quad (28)$$

Fig. 8 shows a comparison of the AdWAF model (a fine solid line with circle) and the K lens (a bold solid line), in condition of $r_{\max} = 1$, $\theta_{\max} = 60°$, $\theta_0 = 2.584°$, $\theta_1 = 20.0°$, and $\theta_2 = 34.715°$ (these values are determined from the specification of the actual K lens). The FE lens (a fine broken line) and the PHC lens (a bold broken line) are also compared with them. This condition of boundaries indicates that the AdWAF image gives us a higher magnification in $0 \le \theta \le \theta_0$ than the K lens when both have the same FOV. On the other hand, when it has the same magnification in the fovea ($0 \le \theta \le \theta_0$), as the K lens does, $r_{\max}$ is 0.85. This means that the AdWAF image reduces the number of pixels by about 28%.

B. Unidirectional Property of the AdWAF Model

Foveation contributes to concentrating attention on the central FOV of an acquired image. That is, the fovea sensor observes an environment nonuniformly by weighting the direction along its optical axis. The author calls this a unidirectional property. The fovea sensor is a unidirectional sensor, compared to the omnidirectional sensor that does uniformly around its optical axis by 360° view. Fig. 9 compares three types foveation models,

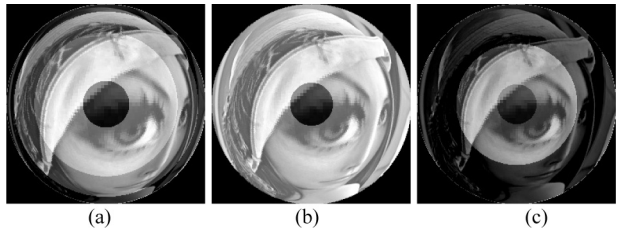

Fig. 9. AdWAF image, LP lens image, and K lens image when $r_{\max} = 64$, $\theta_{\max} = 60°$, $\theta_0 = 2.584°$, $\theta_1 = 20.0°$, and $\theta_2 = 34.715°$. (a) AdWAF image. (b) LP lens image. (c) K lens image.

Fig. 10. Three target images with different scales ($\alpha = 0.75$, 1, and 1.5). (a) $\alpha = 0.75$ (b) $\alpha = 1.0$. (c) $\alpha = 1.5$.

i.e., the AdWAF image, the LP lens image, and the K lens image, simulated in condition of $\theta_{\max} = 60°, \theta_0 = 2.584°, \theta_1 = 20.0°$, and $\theta_2 = 34.715°$, by changing intensity. The FOV is divided into four areas, i.e., fovea (the central dark part), para-fovea (the brightest part), near-periphery (the second brightest part), and periphery (outer dark part). It is noted that the LP lens image has only fovea and para-fovea, and the K lens image does not have para-fovea. The AdWAF image shows higher magnification than the K lens image in the fovea, as mentioned in Section III-A.

Fig. 10 shows three Cartesian target images with different scales ($\alpha = 0.75$, 1, and 1.5). Fig. 11 compares polar images of the AdWAF image (left), the LP lens image (middle), and the K lens image (right), in each scale (in the same condition as in Fig. 9). If some image pattern does not change its shape when it is shifted, we say that it is translation-invariant. With respect to the polar images (see Fig. 11), the pattern in the para-fovea shifts down vertically without changing pattern as the scale α increases. This means that the translation-invariant property in this direction of the polar image is equivalent to the scale-invariant one in the radial direction of the Cartesian image from the image center. Further, rotation around the image center of the Cartesian image (see Fig. 10) corresponds to the horizontal translation-invariant shift in the polar images (see Fig. 11). That is, the polar image has the rotation-invariant property. Therefore, the para-fovea has the rotation- and scale-invariant (RS-invariant) property, i.e., it gives us a log-polar image with the translation-invariant property in the vertical (corresponding to radial) and horizontal (corresponding to tangential) directions, when the image height r is linear to the logarithm of the object height h. On the other hand, it is noted that the near-periphery gives us another log-polar image with the RS-invariant property when r is linear to the logarithm of the incident angle θ.

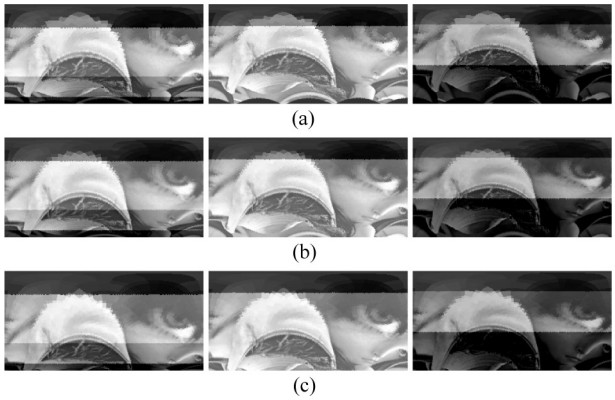

Fig. 11. Polar images of the AdWAF image, LP lens image, and K lens image when $r_{\max} = 64, \theta_{\max} = 60^\circ, \theta_0 = 2.584^\circ, \theta_1 = 20.0^\circ$, and $\theta_2 = 34.715^\circ$. (a) $\alpha = 0.75$ (b) $\alpha = 1.0$. (b) $\alpha = 1.5$.

In order to estimate the scale-invariant property, a length Δr on the image plane is calculated from the object height h and its 95% height h' [see Fig. 12(a)]. Fig. 12(b) shows Δr versus h, under conditions $r_{\max} = 1$, $\theta_{\max} = 60^\circ$, $\theta_0 = 2.584^\circ$, $\theta_1 = 20.0^\circ$, and $\theta_2 = 34.715^\circ$. A fine solid line with a circle, a broken line, and a bold solid line show the AdWAF model, the LP lens, and the K lens, respectively. If a gradient of these lines is constantly zero, a corresponding part (i.e., a planar logarithmic part) is scale-invariant to the planar projection of the object plane. Thus, the images by the LP lens and the AdWAF model are scale-invariant in $\theta_0 \le \theta \le \theta_{\max}$ and $\theta_0 \le \theta \le \theta_1$, respectively. On the other hand, the *spherical logarithmic* part ($\theta_0 \le \theta \le \theta_1$) of the K lens model is not scale-invariant exactly, i.e., Δr at $\theta_1 = 20.0^\circ$ ($h_1 = 0.21$) decreases by about 7.6% error from Δr at $\theta_0 = 2.584^\circ$ ($h_0 = 0.026$).

Fig. 12(b) shows the K lens curve (a fine solid line without circle), simulated by the AdWAF model, under the condition $\theta_{\max} = 60^\circ$, $\theta_0 = 2.584^\circ$, and $\theta_1 = 34.715^\circ$ (although θ_1 of the actual K lens is 20.0°). Assuming to match the images with different scales using region over the boundary θ_1 of the *spherical logarithmic* part, we can correct the error of scale-invariance more easily, because the fine solid line changes more smoothly than the actual K kens (i.e., more suitable for approximation). This estimation method of the boundaries θ_i gives us a guide for designing the fovea sensor by the AdWAF model.

The fovea of the AdWAF model gives us the translation-invariant property as shown in Fig. 13, because it has uniform magnification based on the *Cartesian planar* projection.

C. Examination of the AdWAF Model by Optical Flow

This section examines the unidirectional property of the AdWAF model using optical flow by comparing with the PHC lens model. Fig. 14(a) and (b) shows optical flow (Δr, $\Delta\phi$) from a point $(u_{i-1},\ v_{i-1})$ at time $t = i - 1$ to a point (u_i, v_i) at $t = i$ on the image plane, and view point coordinates in camera motion. It is assumed that the camera has the AdWAF model or the PHC lens and that the Cartesian target image is set as it is perpendicular to the optical axis of the camera, having a

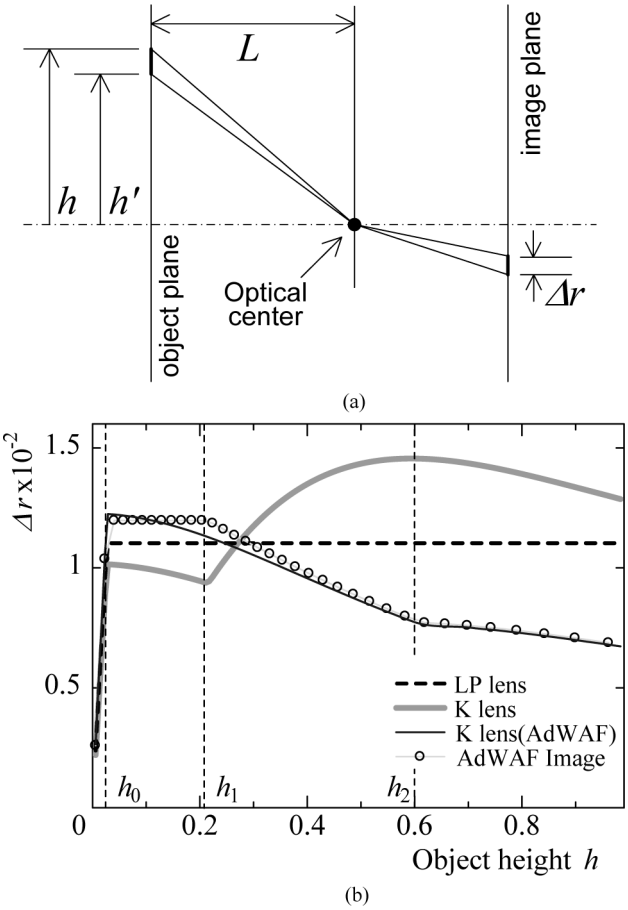

Fig. 12. Scale-invariant property by the AdWAF image, LP lens, and K lens. (a) A sketch of Δr. (b) Δr versus h.

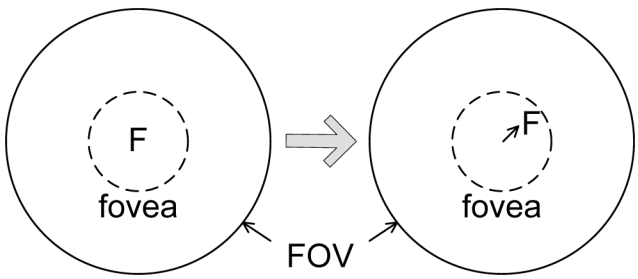

Fig. 13. Translation-invariant property in fovea.

distance L_{i-1} from the camera view point (the optical center) at $t = i - 1$ to the image center (I_u, I_v). Camera view point coordinates (x_i, y_i, z_i) of a point P at $t = i$ are defined from $(x_{i-1}, y_{i-1}, z_{i-1})$ at $t = i - 1$ by taking the camera motion into account as follows:

$$\begin{bmatrix} x_i \\ y_i \\ z_i \end{bmatrix} = \boldsymbol{R}^{-1} \left(\begin{bmatrix} x_{i-1} \\ y_{i-1} \\ z_{i-1} \end{bmatrix} - \boldsymbol{T} \right) \tag{29}$$

where $\boldsymbol{R}$ and $\boldsymbol{T}$ are rotation matrices composed of rotations ψ_x, ψ_y, and ψ_z and translation vector composed of translations T_x, T_y, and T_z, respectively.

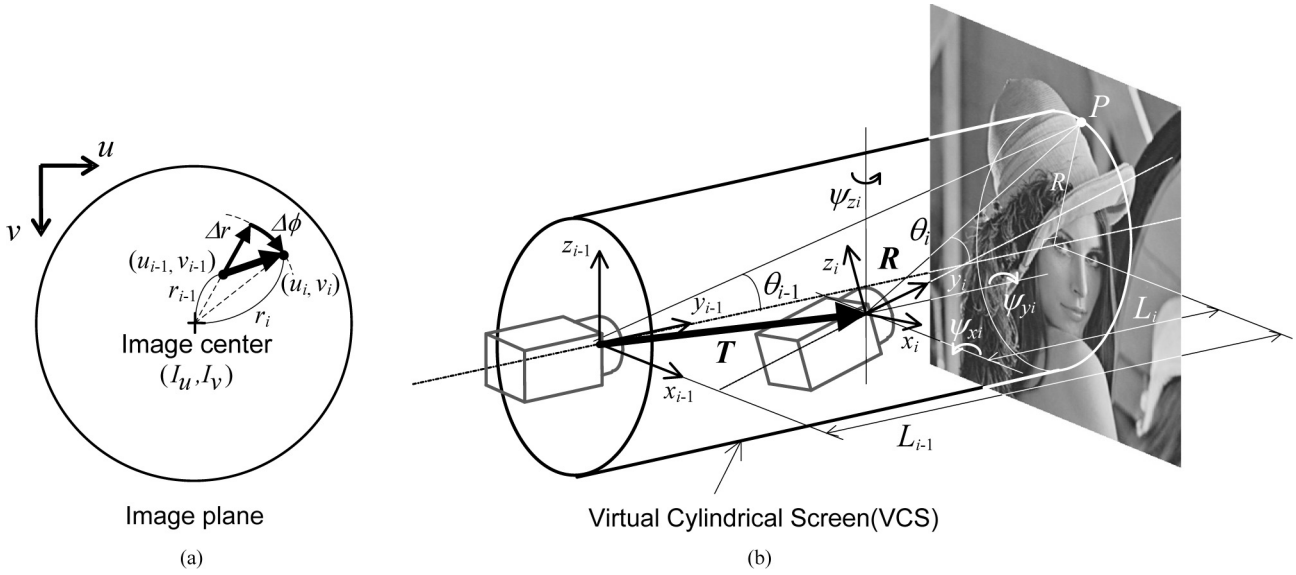

Fig. 14. Calculation of optical flow. (a) Optical flow on the image plane. (b) View point coordinates in camera motion and the virtual cylindrical screen.

Fig. 15 shows the optical flow of the AdWAF model and the PHC lens model when the camera moves laterally from the optical axis, i.e., $\psi_x = \psi_y = \psi_z = 0$, $T_y = T_z = 0$, and $T_x = L_{i-1}/20$. The condition of this simulation is $r_{\max} = 256$ pixel, $\theta_{\max} = 60^\circ$, $\theta_0 = 9.826^\circ$, $\theta_1 = 19.107^\circ$, and $\theta_2 = 34.715^\circ$. Each white line, as drawn in Fig. 15, indicates optical flow, i.e., a vector between two matching points. The distance L_{i-1} is defined in the following equation:

$$L_{i-1} = \frac{r_{\max}}{\tan\theta_{\max}}. \tag{30}$$

The optical flow in the fovea by the AdWAF model is uniform, because this motion corresponds to translation [see Fig. 15(b)]. Thus, the AdWAF model gives us a much wider translation-invariant area due to much higher magnification of the fovea than the PHC lens model.

Fig. 16 shows the optical flow when the camera moves forward along the optical axis, i.e., $\psi_x = \psi_y = \psi_z = 0, T_x = T_z = 0$, and $T_y = L_{i-1}/10$. In this case, a tangential component $\Delta\phi$ of the optical flow is zero ideally [see Fig. 16(d)]. It is noted that the AdWAF model can reduce the variation of a radial component Δr of the optical flow compared to the PHC lens model, where Δr increases rapidly toward the peripheral FOV. The camera motion along the optical axis makes Δr in para-fovea uniform, because this motion corresponds to scaling mentioned in Section III-B. The AdWAF model gives us much wider area, with a scale-invariant property obviously, than the PHC lens model.

Fig. 17 shows that the radial component Δr of the optical flow of the point P on a virtual cylindrical screen (VCS) [see Fig. 14(b)] in the forward motion (i.e., $\psi_x = \psi_y = \psi_z = 0$ and $T_x = T_z = 0$). VCS is set along the optical axis of the camera, having a radius R. The point P shifts on this cylindrical surface in the direction of the optical axis in this simulation. Two cases of $T_y/R = 0.1$ and $T_y/R = 0.2$ are simulated compared to the AdWAF model and the PHC lens model. The radial component Δr is normalized by $r_{\max}$. We note two facts from Fig. 17. The first is that the AdWAF model can reduce the variation of Δr, compared to the PHC lens model, similarly to the case when the point P is on the target image perpendicular to the optical axis. Especially in large incident angles of the periphery, Δr is reduced largely. The second is that the AdWAF model gives us a larger Δr in incident angles from the fovea to the middle of the near-periphery than the PHC lens model. These facts of equalizing and enlarging the motion on the image plane indicate that the AdWAF model is superior to the PHC lens model in terms of computation and application of the optical flow in the forward motion. That is, the optical flow can be computed more reliably when it is determined using some local method, such as a block-matching method [16] and a local gradient method [17].

Fig. 18 shows the optical flow when the camera rotates around the optical axis, i.e., $\psi_x = \psi_z = 0$, $\psi_y = 10^\circ$, and $T_x = T_y = T_z = 0$. In this case, the radial component Δr of the optical flow is zero ideally [see Fig. 18(b) and (d)]. On the other hand, the tangential component $\Delta\phi$ is uniform in the same incident angle in both of the AdWAF model and the PHC lens model. It is noted that the polar images are given a uniform $\Delta\phi$ not only in the para-fovea but also in the entire FOV by this camera motion. This rotation gives us the rotation-invariant property regardless of the types of the image and lens model. In other words, Fig. 18 indicates an important property that the summation of $\Delta\phi$ in the entire FOV is constant in case of any camera model when the camera rotates around the optical axis. This property makes it easier to separate the component of this rotation from the optical flow.

Comparing the lateral motion and the forward/backward motion, it is noted that the AdWAF model calculates larger amount of radial component of the optical flow from the entire FOV in the lateral motion. On the other hand, the PHC lens model has a larger amount in the forward/backward motion. This property shows that the AdWAF model gives us convenience for tracking

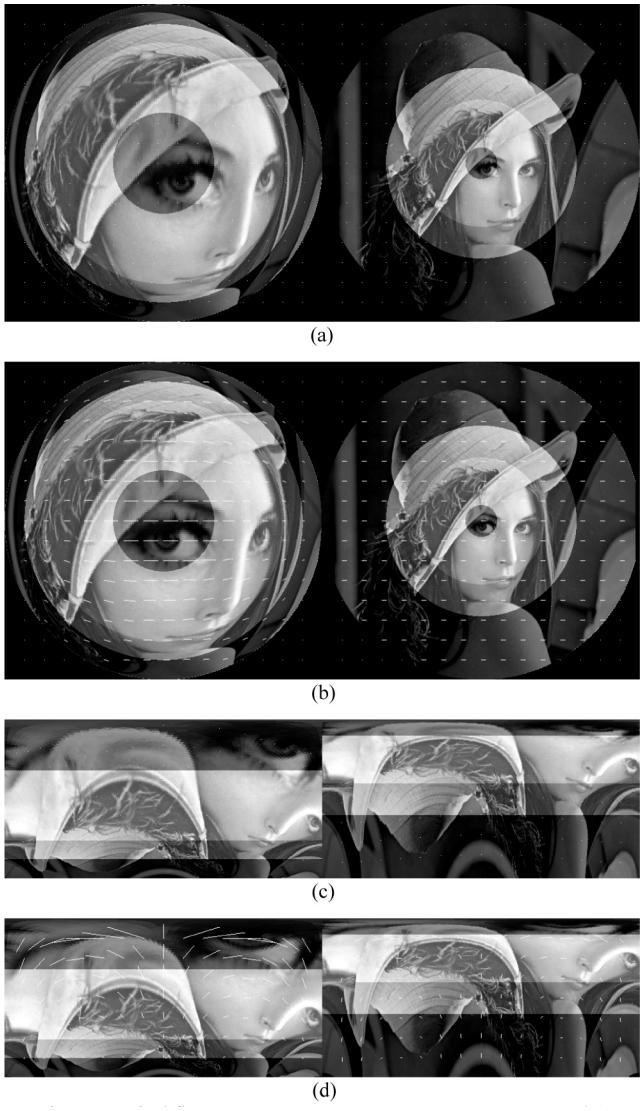

Fig. 15. Optical flow of the AdWAF image (left) and PHC image (right) when the camera moves laterally from the optical axis. (a) AdWAF image and PHC image before camera motion. (b) AdWAF image and PHC image after camera motion. (c) Polar images before camera motion. (d) Polar images after camera motion.

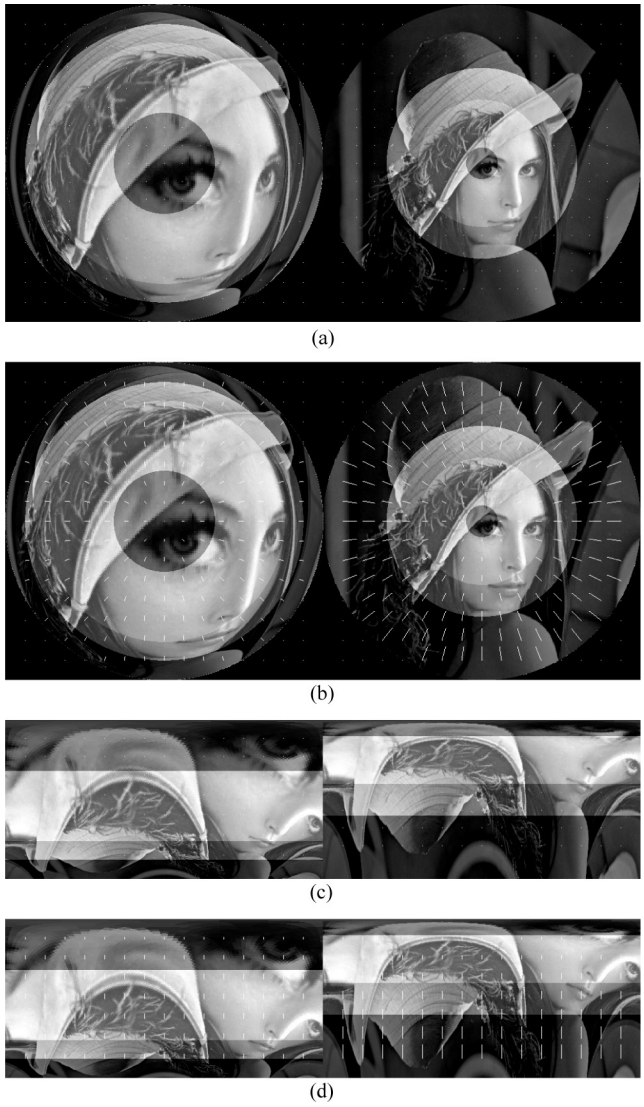

Fig. 16. Optical flow of the AdWAF image (left) and PHC image (right) when the camera moves forward along the optical axis. (a) AdWAF image and PHC image before camera motion. (b) AdWAF image and PHC image after camera motion. (c) Polar images before camera motion. (d) Polar images after camera motion.

at a moving object by focusing on the lateral motion particularly, because it is more sensitive to the lateral motion and more robust to the forward/backward motion. That is, we can detect the lateral motion more easily by foveation even if the camera or the object moves along the optical axis. This advantage should be discussed with other works on active visual tracking using the fovea sensor (or log-polar mapping) [18]–[21]. These previous works compute the optical flow in log-polar coordinates. The advantage of foveation, as mentioned before, can be enhanced by using the fovea lens for the fovea sensor, because the fovea lens can realize higher resolution in the fovea than the vision chip or computational remapping. The author thinks that this property comes from the fact that a foveation model (such as the AdWAF model) is originally inspired from a mechanism of the human vision by which we need to change the attention point in the FOV actively.

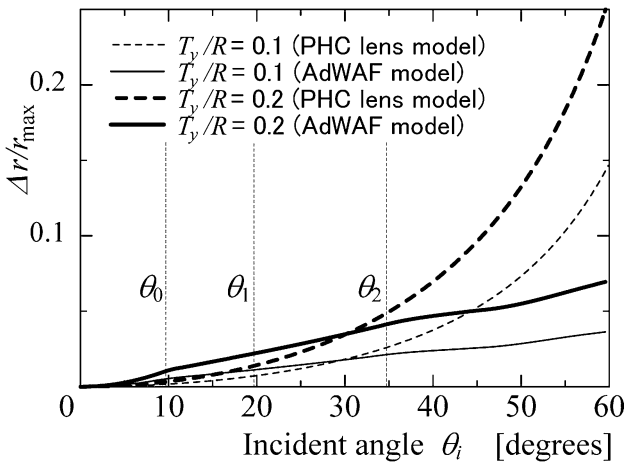

Fig. 17. Optical flow of point P on the virtual cylindrical screen when the camera moves forward along the optical axis.

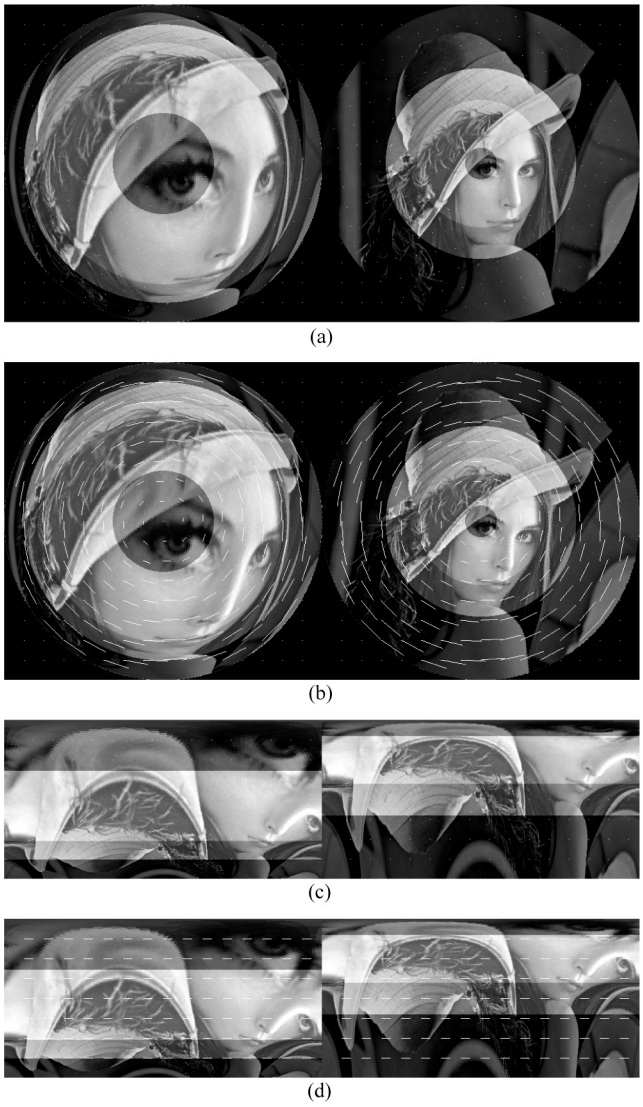

Fig. 18. Optical flow of the AdWAF image (left) and PHC image (right) when the camera rotates abound the optical axis. (a) AdWAF image and PHC image before camera motion. (b) AdWAF image and PHC image after camera motion. (c) Polar images before camera motion. (d) Polar images after camera motion.

IV. Conclusion

This paper proposed a model of a wide-angle space-variant image that provides a guide for designing an actual fovea sensor. The advantages of the proposed model have been estimated and demonstrated by comparing with other models. The main points are summarized as follows.

1) AdWAF model was proposed. The AdWAF model was formulated taking all-purpose use into account. This model divided its wide-angle FOV into four regions by combining Cartesian (linear) coordinates and logarithmic coordinates in both planar projection and spherical projection, so that it could represent the image by various types of lens, flexibly.
2) The simulation results of the image height and resolution showed that the AdWAF model could reduce image data by 13.5%, compared with a log-polar lens model, when both the models had the same resolution in the central FOV.
3) It was demonstrated that the image by the AdWAF model could be remapped from an actual input image by the prototype fovea lens.
4) Other foveation models used for the existing log-polar chip and vision system had been discussed. The AdWAF model could represent these models.
5) The AdWAF model had the translation-invariant property in the fovea and the scale-invariant property in the para-fovea. This model gave its planar logarithmic part a complete scale-invariant property, while Kuniyoshi lens (K lens) had 7.6% error at the most in its spherical logarithmic part.
6) The foveation model such as the AdWAF model detected the lateral motion more easily than the PHC lens model, using the optical flow, when the camera or the object moved along the optical axis.
7) The fovea sensor by the special wide-angle lens enhanced the advantage of 6).
8) Summation of the tangential component of optical flow in the entire FOV was constant in case of any camera model when the camera rotated around the optical axis.

Many industrial applications of vision sensing require a wide-angle FOV and high resolution at the same time for image processing, surveillance, and monitoring [11]–[13]. It is expected that the wide-angle fovea sensor break through a tradeoff between the wide-angle FOV and high resolution of the existing image sensor without increasing the data.

Acknowledgment

The author thanks G. Sandini and F. Berton, a Professor and a Researcher in the Laboratory for Integrated Robotics (LIRA), University of Genova, Italy, for collaboration, and sincerely says best regards to H. Jiang and J. W. Burdick, a Ph.D. student and a Professor at the California Institute of Technology.

References

[1] S. Shimizu, "Multi-functional application of wide angle foveated vision sensor in mobile robot navigation," *J. Robot. Mechatronics*, vol. 14, no. 4, pp. 382–389, Aug. 2002.
[2] E. L. Schwartz, "Spatial mapping in the primate sensory projection: Analytic structure and relevance to perception," *Biol. Cybern.*, vol. 25, no. 4, pp. 181–194, Dec. 1977.
[3] G. Sandini and V. Tagliasco, "An anthropomorphic retina-like structure for scene analysis," *Comput. Graph. Image Process.*, vol. 14, no. 4, pp. 365–372, Dec. 1980.
[4] F. Berton, G. Sandini, and G. Metta, "Anthropomorphic visual sensors," in *Encyclopedia of Sensors,* vol. 10, C. A. Grimes, E. C. Dickey, and M. V. Pishko, Eds. Stevenson Ranch, CA: Amer. Sci. Publishers, 2005, pp. 1–16.
[5] J. Van Der Spiegel, G. Kreider, C. Claeys, I. Debusschere, G. Sandini, P. Dario, F. Fantini, P. Belluti, and G. Soncini, "A foveated retina-like sensor using CCD technology," in *Analog VLSI Implementations of Neural Networks*, C. Mead and M. Ismail, Eds. Boston, MA: Kluwer, May 1989.
[6] R. Wodnicki, G. W. Roberts, and M. D. Levine, "A foveated image sensor in standard CMOS technology," in *Proc. Custom Integr. Circuits Conf.*, Santa Clara, CA, May 1995, pp. 357–360.
[7] S. Shimizu and R. Suematu, "Vision sensor with wide angle and high distortion lens," in *Video Proc. IEEE Int. Conf. Robot. Autom., Visual Sensing 3*, Nagoya, Japan, May 1995, pp. 893–900.

[8] Y. Kuniyoshi, N. Kita, K. Sugimoto, S. Nakamura, and T. Suehiro, "A foveated wide angle lens for active vision," in *Proc. IEEE Int. Conf. Robot. Autom.*, Nagoya, Japan, May 1995, pp. 2982–2988.
[9] S. Shimizu, H. Jiang, and J. W. Burdick, "Image extraction by wide angle foveated lens for overt-attention," in *Proc. IEEE Int. Conf. Robot. Autom.*, Orlando, FL, May 2006, pp. 3437–3442.
[10] S. Shimizu, R. Suematu, and S. Yahata, "Wide-angle vision sensor with high-distortion lens (detection of camera location and gaze direction based on the two-parallel-line algorithm)," *JSME Int. J. Ser. C*, vol. 41, no. 4, pp. 893–900, Dec. 1998.
[11] R. Stanciu and C. Y. Oh, "Human-in-the-loop camera control for a mechatronic broadcast boom," *IEEE/ASME Trans. Mechatronics*, vol. 12, no. 1, pp. 41–52, Feb. 2007.
[12] J. S. Hu and T. M. Su, "Robust environmental change detection using PTZ camera via spatial-temporal probabilistic modeling," *IEEE/ASME Trans. Mechatronics*, vol. 12, no. 3, pp. 339–344, Jun. 2007.
[13] K. Suzumori, T. Miyagawa, M. Kimura, and Y. Hasegawa, "Micro inspection robot for 1-in pipes," *IEEE/ASME Trans Mechatronics*, vol. 4, no. 3, pp. 286–292, Sep. 1999.
[14] M. Bolduc and M. D. Levine, "A review of biologically-motivated space-variant data reduction models for robotic vision," *Comput. Vis. Image Understanding*, vol. 69, no. 2, pp. 170–184, Feb. 1998.
[15] S. W. Wilson, "On the retino-cortical mapping," *Int. J. Man-Mach. Stud.*, vol. 18, no. 4, pp. 361–389, 1983.
[16] J. Jain and A. Jain, "Displacement measurement in its application in interframe image coding," *IEEE Trans. Commun.*, vol. 29, no. 12, pp. 1799–1808, Dec. 1981.
[17] B. K. P. Horn and B. G. Schunck, "Determining optical flow," *Artif. Intell.*, vol. 17, pp. 185–203, 1981.
[18] A. Bernardino, J. Santos-Victor, and G. Sandini, "Foveated active tracking with redundant 2D motion parameters," *Robot. Auton. Syst.*, vol. 39, pp. 205–221, Jun. 2002.
[19] F. Panerai, C. Capurro, and G. Sandini, "Space variant vision for an active camera mount," in *Proc. SPIE–Visual Inf. Process. IV*, Jun. 1995, vol. 2488, pp. 284–296.
[20] C. Capurro, F. Panerai, and G. Sandini, "Space variant vision for an active camera mount," *Int. J. Comput. Vis.*, vol. 24, no. 1, pp. 79–94, Aug. 1997.
[21] A. Bernardino and J. Santos-Victor, "Binocular tracking: Integration of perception and control," *IEEE Trans. Robot. Autom.*, vol. 15, no. 6, pp. 1080–1094, Dec. 1999.

Sota Shimizu (M'05) was born in Nagoya, Japan, in 1970. He received the Ph.D. degree in electronic–mechanical engineering from Nagoya University, Nagoya, in 1998.

From 1998 to 1999, he was with Nagoya University. From 2000 to 2002, he was with Tokai University as an Assistant Professor. Since 2003, he has been with the California Institute of Technology, Pasadena. His current research interests include cognitive vision, sensing, robot vision, and signal processing. He has participated in several national and international research projects. He has authored or coauthored several articles in international journals and conference proceedings.